PIECE-WISE CAUSAL INVERSION BY OUTPUT REDEFINITION FOR A FLEXIBLE LINK MANIPULATOR

M. Vakil, R. Fotouhi*, P. N. Nikiforuk
Department of Mechanical Department, University of Saskatchewan, 57 Campus Drive, Saskatoon, S7N 5A9, Saskatchewan, Canada
E-mail: reza.fotouhi@usask.ca

Received July 2008, Accepted February 2009
No. 08-CSME-26, E.I.C. Accession 3064

ABSTRACT

A new causal dynamic end-effector inversion method for a single flexible link manipulator is introduced. Contrary to the available non-causal inversion technique, this method does not lead to pre-actuation and works even in the presence of the purely imaginary zeros for the transfer function. Based on this approach, the desired end-effector trajectory is divided into a finite number of segments. In each segment, the desired trajectory is redefined so that a bounded continuous torque through causal dynamic inversion is obtained. The redefinition of the desired trajectory at each segment employs summation of stable exponential functions. This leads to a family of answers for the redefined trajectory, which is an advantage for control engineers. The results of the simulation and experimental studies show the feasibility and effectiveness of this new technique.

INVERSION CAUSALITE « PIECE-WISE» PAR SORTIE REDÉFINIE POUR UN LIEN DE MANIPULATEUR SOUPLE

RÉSUMÉ

Une nouvelle méthode de dynamique de causalité pour l'inversion de l'effecteur est introduite pour un manipulateur flexible à une seule membrure. Contrairement aux méthodes couramment publiées de technique de non-inversion de causalité, cette nouvelle méthode ne conduit pas au pré-déclenchement et fonctionne même en présence que des zéros imaginaires pour la fonction de transfert. À partir de cette méthode, la trajectoire désirée pour l'effecteur est divisée en un nombre fini de segments. Dans chaque segment, la trajectoire désirée est redéfinie de telle sorte qu'un couple continue bornée est obtenue par inversion de causalité dynamique. La redéfinition de la trajectoire souhaitée sur chaque segment utilise l'addition de fonctions exponentielles stables. Cette méthode conduit à une famille de réponses pour la redéfinition de la trajectoire qui est un avantage pour les ingénieurs de contrôle. Les résultats de la simulation et les études expérimentales montrent la faisabilité et l'efficacité de cette nouvelle technique.

1. INTRODUCTION

Smaller mass, lower peak power and less energy consumption are among the main potential advantages of Flexible Link Manipulators (FLM) over rigid link manipulators. However, their general performance is not as good as that of rigid link manipulators. To improve the general performance of FLM, much research has been carried out during the past decade; in particular, because of the importance of End-Effector Trajectory Tracking (EETT), many of these studies have been focused on the EETT of FLM. The challenging aspect of the research, the EETT of FLM, is due to the fact that the system is non-minimum phase [1]. The non-minimum phase property is the consequence of the flexibility of the link and the non-collocation of the sensor and actuator [2,3].

A possible approach for the EETT of FLM is the use of the output regulation technique introduced in [4]. The feasibility of applying this method to FLM was studied in [5]. To apply this method, the nontrivial solution for a set of first order partial differential equations is required. Moreover, for the EETT of a FLM which has non-minimum phase characteristics, the application of the method introduced in [4] leads to transient errors at the initial and final portions of the manoeuvre [6]. Another alternative for the EETT of a FLM is the use of stabilizing feedback (on-line signal indicated by 2 in Fig. 1) with the feedforward command (off-line signal indicated by 1 in Fig. 1) created by the inversion of the system dynamic. Due to the non-minimum phase property of the system, bounded causal inversion of the dynamic equation for a desired end-effector trajectory is not achievable [7 Ch. 6]. However, for a linear model of a Single Flexible Link Manipulator (SFLM), the non-causal inversion of the dynamic equations for a desired end-effector trajectory was introduced in [8,9] and the extension of the method to general nonlinear systems was studied in [6]. Rather than the non-causal input torque, in [10] a method was proposed that creates a causal end-effector inversion for a SFLM through rest-to-rest and point-to-point motion planning. In general, however, it is more desirable to invert the dynamic equations for the desired end-effector trajectory rather than planning a point-to-point and rest-to-rest motion.

In this paper a causal end-effector trajectory inversion by the output redefinition for a SFLM is introduced. This new causal method, unlike the available non-causal inversion technique [8,9] which does not tolerate the existence of purely imaginary zeros [11], works even if the transfer function of the system has purely imaginary zeros. To utilize this new technique, the desired end-effector trajectory is divided into several segments and is redefined in each segment by the Summation of Stable Exponential Functions (SSEF) [12], that is:

$$\tilde{y}_d(t) = \sum_{j=0}^{r} c_j e^{m_j t},\ m_j < 0 \tag{1}$$

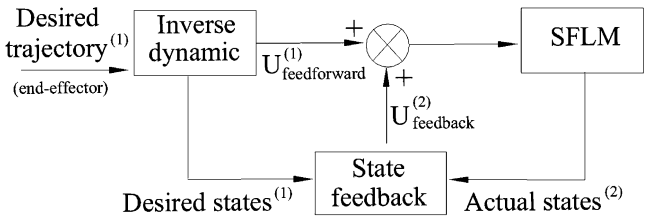

Fig. 1. Schematic of the end-effector trajectory tracking method, $\{.\}^1$: off-line signal, $\{.\}^2$: on-line signal

Here $\tilde{y}_d(t)$ is the redefined end-effector trajectory and c_j ($j = 1, \ldots, r$) are constants which are calculated, after the selection of the r and m_j, so that a bounded continuous torque through causal inversion is possible. To clarify the concept an example is provided in Section 4. There are four steps to this approach, which are explained in Section 5. Also a method for the selection of r and m_j is introduced in Section 6.

Comparing the SSEF with a polynomial function having r terms, the same number of terms as the SSEF,that is:

$$y_p(t) = \sum_{j=0}^{r} p_j t^j \tag{2}$$

it can be seen that the number of the choices available using SSEF, c_j and m_j in Eq. (1), is twice the number of choices available in the polynomial, p_j in Eq. (2). Therefore, while for a predefined set of conditions equal to the number of coefficients in $y_p(t)$ there is only one solution set for the polynomial function, for the same conditions there is a family of possible solution for $\tilde{y}_d(t)$ in SSEF. Hence, the control engineer finds the family member of the redefined trajectories that best meets the required design criteria.

It should be mentioned that the method introduced in this paper is only applicable to linear systems or linearized systems, for example a linear SFLM. Thus, it cannot be extended to manipulators with multi-links where the dynamic equations are nonlinear. Moreover this method is different than the Rayleigh-Ritz (RR) method. In the RR method, a descritized dynamic model for a continuous system (e.g a SFLM) will be found while the output redefinition introduced in this paper finds a causal end-effector inversion for a nonminimum phase SFLM.

2. DYNAMIC MODELING OF A SFLM

In this paper, to find the dynamic equations of a SFLM the Lagrange equation is combined with the Assumed Mode shape Method (AMM) approximation [13,14]. In the AMM the spatial deflection of the flexible link, $\xi(\gamma,t)$ in Fig. 2, is described by a finite series composed of spatial pre-defined shape functions, $\phi_j(\gamma)$, multiplied by the time varying weight functions, $\lambda_j(t)$. Therefore:

$$\xi(\gamma,t) = \sum_{j=1}^{n} \phi_j(\gamma)\lambda_j(t) \tag{3}$$

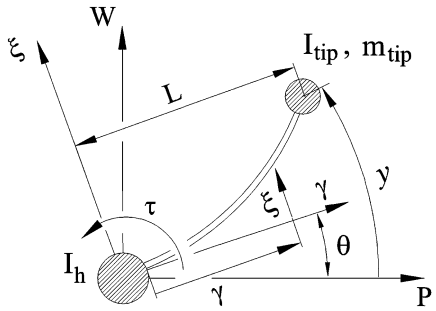

Fig. 2. Schematic of a SFLM, P-W: Inertial coordinate frame, γ–ξ: Rotating coordinate frame, y: Length of the arc of the end-effector displacement

where n is the number of the assumed mode shapes, $\phi_j(\gamma)$ is the jth mode shape which was adopted from [14], t is time and γ is measured along the axial rotating coordinate as shown in Fig. 2.

After deriving the kinetic and potential energies of a SFLM and by using the Lagrange equations with the consideration that θ and λ_j ($i = 1 \ldots n$) are the generalized coordinates, the dynamic equations of a SFLM are:

$$\mathbf{M}(\boldsymbol{\lambda})\ddot{\boldsymbol{q}} + \mathbf{C}_{\mathbf{cc}}(\dot{\theta},\boldsymbol{\lambda},\dot{\boldsymbol{\lambda}})\dot{\boldsymbol{q}} + \mathbf{K}_B\boldsymbol{q} = \boldsymbol{F} \tag{4}$$

where $\boldsymbol{q} = \begin{bmatrix} \theta & \boldsymbol{\lambda}^T \end{bmatrix}^T$, $\boldsymbol{\lambda} = \begin{bmatrix} \lambda_1 & \lambda_2 & \ldots & \lambda_n \end{bmatrix}^T$, $\mathbf{M}(\boldsymbol{\lambda})$ is the mass matrix, $\mathbf{C}_{\mathbf{cc}}(\dot{\theta},\boldsymbol{\lambda},\dot{\boldsymbol{\lambda}})$ is the matrix representing the Coriolis force and the component of the centrifugal force in the lateral direction, and $\mathbf{K}_\mathrm{B}$ is the stiffness matrix. Moreover, $\boldsymbol{F}$ is the force vector which is:

$$\boldsymbol{F} = \boldsymbol{H}\tau \tag{5}$$

where τ is the input torque and $\boldsymbol{H} = \begin{bmatrix} 1 & 0_{1\times n} \end{bmatrix}^T$. Details of Eq. (4) can be found in Chapter 2 in [15]. Eq. (4) is a nonlinear equation; however assuming small lateral deflection and thus neglecting the nonlinearities, the linear equation of a SFLM is:

$$\mathbf{M}\ddot{\boldsymbol{q}} + \mathbf{K}_B\boldsymbol{q} = \boldsymbol{H}\tau \tag{6}$$

where $\mathbf{M}$ is constant contrary to $\mathbf{M}(\boldsymbol{\lambda})$ in Eq. (4). Finally, considering the material damping and using the Rayleigh damping model, the damping matrix $\mathbf{C}_\mathrm{D}$ is:

$$\mathbf{C}_D = (2\eta/\omega)\mathbf{K}_B \tag{7}$$

where η and ω are the damping ratio and natural frequency of the fundamental vibration mode shape, respectively. Thus, the linear model of a SFLM is:

$$\mathbf{M}\ddot{\boldsymbol{q}} + \mathbf{C}_D\dot{\boldsymbol{q}} + \mathbf{K}_B\boldsymbol{q} = \boldsymbol{H}\tau \tag{8}$$

3. END-EFFECTOR INVERSION PROCEDURE

The linear dynamic model of a SFLM, Eq. (8), considering the base torque as the input and the end-effector displacement as the output can be written as:

$$\begin{cases} \dot{\boldsymbol{X}} = \mathbf{A}\boldsymbol{X} + \boldsymbol{B}\tau & (9a) \\ y = \boldsymbol{C}\boldsymbol{X} & (9b) \end{cases}$$

where

$$\boldsymbol{X} = \begin{bmatrix} \boldsymbol{q} \\ \dot{\boldsymbol{q}} \end{bmatrix}, \mathbf{A} = \begin{bmatrix} 0_{n+1\times n+1} & \mathbf{I}_{n+1\times n+1} \\ -\mathbf{M}^{-1}\mathbf{K}_B & -\mathbf{M}^{-1}\mathbf{C}_D \end{bmatrix}, \boldsymbol{B} = \begin{bmatrix} 0_{n+1\times 1} \\ \mathbf{M}^{-1}\boldsymbol{H} \end{bmatrix},$$
$$\boldsymbol{C} = \begin{bmatrix} \boldsymbol{D} & 0_{1\times n+1} \end{bmatrix}, \boldsymbol{D} = \begin{bmatrix} L & \phi_1(L) & \ldots & \phi_n(L) \end{bmatrix} \tag{10}$$

and y is shown in Fig. 2.

For the purpose of inversion the output y has to be differentiated twice [8,9] so that the input τ appears explicitly (See [15] for more details). Thus, differentiating y in Eq. (9b) twice leads to:

$$\ddot{y} = \boldsymbol{C}\mathbf{A}^2\boldsymbol{X} + \boldsymbol{C}\mathbf{A}\boldsymbol{B}\tau \tag{11}$$

Using the input-output linearization technique ([7] Ch. 6.1.3 and 6.4), the base torque has to be:

$$\tau_I = (1/\boldsymbol{C}\mathbf{A}\boldsymbol{B})(\ddot{y}_d - \boldsymbol{C}\mathbf{A}^2\boldsymbol{X}) \tag{12}$$

where y_d is the desired end-effector trajectory and, for a SFLM, the scalar value $\boldsymbol{C}\mathbf{A}\boldsymbol{B} \neq 0$. Thus, replacing τ in Eq. (11) with the torque τ_I given in Eq. (12), results in:

$$\ddot{y} = \ddot{y}_d \tag{13}$$

However, since the order of this inversed system, Eq. (13), is two and the order of the original system, Eq. (9a), is $2(n+1)$ there is an internal dynamics of order $2(n+1) - 2$ as pointed out in [7]. This internal dynamic is:

$$\dot{\boldsymbol{X}}_I = \mathbf{A}_I\boldsymbol{X}_I + \boldsymbol{B}_I\ddot{y}_d \tag{14}$$

where $\boldsymbol{X}_I = \begin{bmatrix} \lambda_1 & \ldots & \lambda_n & \dot{\lambda}_1 & \ldots & \dot{\lambda}_n \end{bmatrix}^T$ and the definition of $\mathbf{A}_I$ and $\mathbf{B}_I$ as well as the details to derive this internal dynamics are given in [15].

After the inversion procedure, since $\boldsymbol{X} = \mathbf{T}^{-1}\begin{bmatrix} y_d & \dot{y}_d & \boldsymbol{X}_I^T \end{bmatrix}^T$ (see the definition of constant matrix $\mathbf{T}$ in [15]), if $\boldsymbol{X}_I$ is bounded from Eq. (14) (for a bounded $\ddot{y}_d$), $\boldsymbol{X}$ is also bounded. Thus, the inversion torque from Eq. (12) is bounded. However, because SFLM is a non-minimum phase system, some of the eigenvalues of $\mathbf{A}_I$ in Eq. (14) have positive real parts ([7] Ch. 6.1.3, [8], [9]) and thus the internal dynamics is unstable. This means that the feedforward integration of Eq. (14), for a bounded $\ddot{y}_d$, generally leads to an unbounded response for $\boldsymbol{X}_I$. In this paper, to have a bounded response for $\boldsymbol{X}_I$, y_d is redefined so that the causal integration of Eq. (14) assures a bounded $\boldsymbol{X}_I$.

4. CAUSAL INVERSION BY OUTPUT REDEFINITION

By transformation Eq. (14) can be written as (details can be found in [15]):

$$\begin{bmatrix} \dot{\boldsymbol{X}}_I^s \\ \dot{\boldsymbol{X}}_I^u \end{bmatrix} = \begin{bmatrix} \mathbf{A}_I^- & \mathbf{0} \\ \mathbf{0} & \mathbf{A}_I^+ \end{bmatrix} \begin{bmatrix} \boldsymbol{X}_I^s \\ \boldsymbol{X}_I^u \end{bmatrix} + \begin{bmatrix} \boldsymbol{B}_I^s \\ \boldsymbol{B}_I^u \end{bmatrix} \ddot{y}_d \tag{15}$$

where $\mathbf{A}_I^-$ ($\mathbf{A}_I^+$) is a diagonal matrix with the diagonal elements that are the eigenvalues of $\mathbf{A}_I$ with negative (positive) real parts. Also, if $\mathbf{A}_I$ has purely imaginary eigenvalues, the corresponding diagonal matrix, will be included in $\mathbf{A}_I^+$. Due to the existence of $\mathbf{A}_I^+$, the causal integration of Eq. (15) generally results in an unbounded response for $\boldsymbol{X}_I^u$ and thus $\boldsymbol{X}_I$ will be unbounded. For a given set of initial condition(s) to have a bounded causal $\boldsymbol{X}_I^u$, the desired acceleration $\ddot{y}_d$, is replaced by its redefinition, $\tilde{\ddot{y}}_d$, so that the causal solution for:

$$\dot{\boldsymbol{X}}_I^u = \mathbf{A}_I^+\boldsymbol{X}_I^u + \boldsymbol{B}_I^u\tilde{\ddot{y}}_d \tag{16}$$

is bounded. Moreover after finding bounded $\boldsymbol{X}_I^u$ from Eq. (16), the bounded $\boldsymbol{X}_I^s$ can be calculated by the feedforward integration of:

$$\dot{\boldsymbol{X}}_I^s = \mathbf{A}_I^- \boldsymbol{X}_I^s + \boldsymbol{B}_I^s \tilde{\ddot{\boldsymbol{y}}}_d \tag{17}$$

Having $\boldsymbol{X}_I^u$ and $\boldsymbol{X}_I^s$ for the redefined acceleration $\tilde{\ddot{\boldsymbol{y}}}_d$, the bounded $\boldsymbol{X}_I$ and thus the bounded $\boldsymbol{X} = \mathbf{T}^{-1}\left[\tilde{y}_d \quad \dot{\tilde{y}}_d \quad \boldsymbol{X}_I^T\right]^T$ can be calculated (See [15] for the definition of $\mathbf{T}$). Consequently, from Eq. (12), the required causal torque for the inversion of $\tilde{y}_d$ will be obtained. To clarify the basic concept of calculating a bounded $\boldsymbol{X}_I^u$ by output redefinition, the following example is provided.

Example: *Find the bounded X_I^u by the output redefinition for $\dot{X}_I^u - aX_I^u = b\ddot{y}_d$ $a>0$*

Without loss of generality, it is assumed that the following differential equation has to be solved for scalar X_I^u:

$$\dot{X}_I^u - aX_I^u = b\ddot{y}_d \quad a>0 \tag{18}$$

where $a > 0$ and b are arbitrary constants and $\ddot{y}_d$ is the acceleration of the desired trajectory. Also it is assumed that the initial condition on X_I^u is:

$$X_I^u(0) = X_0 \tag{19}$$

The complete answer of X_I^u from Eq. (18) is composed of two parts, the particular part $(X_I^u)_p$, and the complementary part $(X_I^u)_c$, that is:

$$X_I^u = (X_I^u)_c + (X_I^u)_p \tag{20}$$

The particular part $(X_I^u)_p$ depends on $\ddot{y}_d$ and can be found by the convolution integral. The complementary part $(X_I^u)_c$ is:

$$(X_I^u)_c = se^{at} \tag{21}$$

where s is constant and will be found from the initial condition and excitation function $\ddot{y}_d$. Since $a > 0$ if $s \neq 0$, $(X_I^u)_c$ is unbounded; thus, generally an unbounded X_I^u will exist. To have a bounded X_I^u the desired acceleration $\ddot{y}_d$, is replaced by its redefinition $\tilde{\ddot{y}}_d$, in Eq. (18) such that:

(*i*)- The constant s in Eq. (21) is zero; and

(*ii*)- The particular solution $(X_I^u)_p$, corresponding to $\tilde{\ddot{y}}_d$, is bounded and satisfies the initial condition $X_I^u(0) = X_0$, given in Eq. (19). For this purpose, $\ddot{y}_d$ is redefined by:

$$\tilde{\ddot{y}}_d = \sum_{j=1}^{r} c_j e^{m_j t} \quad m_j < 0 \tag{22}$$

Replacing $\ddot{y}_d$ in Eq. (18) with $\tilde{\ddot{y}}_d$ results in:

$$\dot{X}_I^u - aX_I^u = b\tilde{\ddot{y}}_d \tag{23}$$

Moreover, in order for the redefined acceleration $\tilde{\ddot{y}}_d$, to have the same values as the desired acceleration $\ddot{y}_d$ at zero time and the final time t_f, the following conditions must be satisfied:

$$\tilde{\ddot{y}}_d(0) = \ddot{y}_d(0),\ \tilde{\ddot{y}}_d(t_f) = \ddot{y}_d(t_f) \tag{24}$$

The complete answer of X_I^u for Eq. (23) is given in Eq. (20), where $(X_I^u)_c$ is given in Eq. (21), and $(X_I^u)_p$ for the redefined acceleration $\tilde{\ddot{y}}_d$, is:

$$(X_I^u)_p = \sum_{j=1}^{r} \frac{bc_j}{m_j - a} e^{m_j t} \tag{25}$$

Thus, by selecting $m_j < 0$ and $m_j \neq a$, $(X_I^u)_p$ is bounded. To have a bounded solution for X_I^u, $(X_I^u)_c$ must then be zero, which means that $s = 0$. Therefore, assuming that the m_j in Eq. (25) are known, (a method for the selection of m_j is given in Section 6) the unknowns c_j are chosen to make $s = 0$. To have a unique solution for c_j, the number of conditions, Eqs. (19) and (24), which is three, have to be the same as the number of the unknowns c_j. Therefore, $r = 3$ and to force $s = 0$, the c_j ($j = 1, \ldots, 3$) is calculated from:

$$\bar{\boldsymbol{c}}_k = \mathbf{Z}_k^{-1} (\boldsymbol{C}_T)_k \tag{26}$$

$$\mathbf{Z}_k = \begin{bmatrix} \dfrac{b}{m_1 - a} & \dfrac{b}{m_2 - a} & \dfrac{b}{m_3 - a} \\ 1 & 1 & 1 \\ e^{m_1 t_f} & e^{m_3 t_f} & e^{m_3 t_f} \end{bmatrix}, \bar{\boldsymbol{c}}_k = \begin{bmatrix} c_1 \\ c_2 \\ c_3 \end{bmatrix}, (\boldsymbol{C}_T)_k = \begin{bmatrix} X_0 \\ \ddot{y}_d(0) \\ \ddot{y}_d(t_f) \end{bmatrix} \tag{27}$$

After finding c_j ($j = 1, \ldots, 3$) for the given m_j ($j = 1, \ldots, 3$) from Eq. (26), $\tilde{\ddot{y}}_d$ is known as given in Eq. (22). In addition, by integrating $\tilde{\ddot{y}}_d$ with respect to time, $\tilde{\dot{y}}_d$ and $\tilde{y}_d$ are also known. As well $X_I^u = (X_I^u)_p$ as given in Eq. (25) and is bounded.

Remark 1: The smaller the error between $\tilde{\ddot{y}}_d$ and $\ddot{y}_d$, the closer will be $\tilde{\dot{y}}_d$ to $\dot{y}_d$ and $\tilde{y}_d$ to y_d. To make $\tilde{\ddot{y}}_d$ closer to $\ddot{y}_d$, one can set the conditions that the time derivatives of the redefined acceleration $\tilde{\ddot{y}}_d$, up to the order h where $h \leq w$, be equal to the original desired acceleration $\ddot{y}_d$, at zero and t_f. This is in addition to the settings given in Eq. (24) and assuming that the desired acceleration is continuous up to the order w.

5. PIECE-WISE TRAJECTORY INVERSION BY OUTPUT REDEFINITION

As explained in Section 4 to calculate the required torque through the end-effector inversion, a bounded response from the internal dynamics, Eq. (14), has to be obtained. Since the input to this internal dynamics is the acceleration of the end-effector trajectory, the desired acceleration $\ddot{y}_d$ is redefined to find a bounded response from the internal dynamics. Furthermore, by dividing the acceleration into several segments the accuracy of the redefinition of the desired trajectory is increased. For the purpose of the trajectory redefinition, the following steps have to be taken:

1- Divide the desired acceleration $\ddot{y}_d$, into several consecutive segments such that:

$$(\ddot{y}_d)_k = \ddot{y}_d,\ t_{ik} \leq t \leq t_{fk},\ k = 1, \ldots, v \tag{28}$$

where v is the number of the segments, t_{ik} and t_{fk} are the initial and final times of the kth segment respectively and $(\ddot{y}_d)_k$ is $\ddot{y}_d$ in the kth segment.

2- In the kth segment, redefine the desired acceleration $(\ddot{y}_d)_k$ by the SSEF, that is:

$$(\tilde{\ddot{y}}_d)_k = \sum_{j=0}^{r} c_{jk} e^{m_{jk} t},\ m_{jk} < 0 \tag{29}$$

The selection of m_{ik} and r will be explained in Section 6.

3- Find the contribution of each exponential function, c_{ik}, for the kth segment such that the following three conditions are met:

3–1- Assuming that the original desired acceleration is continuous up to order w, that is $\ddot{y}_d \in C^w$, the values of the redefined acceleration and its derivatives up to order h, where $h \leq w$, at the beginning and end of each segment are equal to values of the original desired acceleration, that is : (see remark 1):

$$\begin{aligned} &(\tilde{\ddot{y}}_d)_k\big|_{t_{ik}} = (\ddot{y}_d)_k\big|_{t_{ik}}, \ldots\ldots, (\tilde{\ddot{y}}_d)_k^{(h)}\Big|_{t_{ik}} = (\ddot{y}_d)_k^{(h)}\Big|_{t_{ik}} \\ &(\tilde{\ddot{y}}_d)_k\big|_{t_{fk}} = (\ddot{y}_d)_k\big|_{t_{fk}} \ldots\ldots, (\tilde{\ddot{y}}_d)_k^{(h)}\Big|_{t_{fk}} = (\ddot{y}_d)_k^{(h)}\Big|_{t_{fk}} \end{aligned} \tag{30}$$

(Note that $\ddot{y}^{(h)} = d^h \ddot{y}/dt^h = d^{(h+2)} y/dt^{(h+2)}$)

To have a continuously differentiable $(\tilde{\ddot{y}}_d)_k$ and consequently a smooth inverse torque from Eq. (12), $h \geq 1$. Moreover, the greater the h, the closer will be the redefined trajectory to the desired trajectory at the expense of more computational effort. In the simulation and experimental study $h=2$ is selected so that not only $(\tilde{\ddot{y}}_d)_k$ becomes continuously differentiable but also the reasonable accuracy for the redefinition is achieved at the acceptable computation effort.

3–2- The complementary part of the solution of Eq. (16) is zero. This condition assures that a bounded solution for the unstable part of the internal dynamics, Eq. (16), exists.

3–3- The continuity of $\boldsymbol{X}_I^u$ at the beginning of each segment is satisfied, which guarantees that $\boldsymbol{X}$ and torque τ_I are continuous. To have a continuous torque from Eq. (12) when $\ddot{y}_d$ is replaced by $\tilde{\ddot{y}}_d$, $\boldsymbol{X}$ and $\tilde{\ddot{y}}_d$ have to be continuous. From Eq. (30), it can be seen that $\tilde{\ddot{y}}_d$ is continuous. Thus, to have a continuous torque, $\boldsymbol{X}$ and consequently $\boldsymbol{X}_I$ has to be continuous. Continuity of $\boldsymbol{X}_I$ requires that $\boldsymbol{X}_I^u$ and $\boldsymbol{X}_I^s$ be continuous. Since $\boldsymbol{X}_I^s$ is calculated by the causal integration of Eq. (17), it is continuous. Thus, if $\boldsymbol{X}_I^u$ is also continuous, then $\boldsymbol{X}_I$ is continuous. Therefore, to have a continuous solution for $\boldsymbol{X}_I^u$ the final value of $\boldsymbol{X}_I^u$ at the kth segment is considered as the initial condition of $\boldsymbol{X}_I^u$ at the $k+1$th segment.

4- After calculating $\tilde{\ddot{y}}_d$ and the corresponding bounded $\boldsymbol{X}_I^u$, find the corresponding $\boldsymbol{X}_I^s$ from Eq. (17).

Finally, having $\boldsymbol{X}_I^u$ and $\boldsymbol{X}_I^s$ for the redefined acceleration $\tilde{\ddot{y}}_d$, the bounded $\boldsymbol{X}_I$, and $\boldsymbol{X} = \mathbf{T}^{-1}\begin{bmatrix} y_d & \dot{y}_d & \boldsymbol{X}_I^T \end{bmatrix}^T$ can be calculated. Then, the required causal torque for the inversion of $\tilde{y}_d$ will be obtained from Eq. (12).

It is to be noted that the causal integration of the inverse dynamic equations when y_d is replaced with $\tilde{y}_d$, will be carried on from t_i to t_f. That is, the inverse dynamic feedforward command in Fig. 1 is only active from t_i to t_f. Therefore, since the feedforward inverse dynamic signal will not be used after t_f, the stability of the inverse dynamic equation for $t > t_f$ is not a concern.

6. SELECTION OF THE VARIABLES (M_{jk}, r) OF THE REDEFINED OUTPUT

If the exact model of the system without any perturbation was available, the introduced inversion method could be used to calculate the required causal torque on-line. However, in the presence of the uncertainty, the required torque is calculated off-line using the nominal dynamic model and a state feedback is added for the robustness (see Fig. 1). Therefore, the end-effector inversion technique introduced here should be done off-line with causal integration. As a result, the selection of m_{jk} for the redefinition of the desired trajectory should also be done off-line which is explained in the following. After the selection of m_{jk} for the kth segment, (explained later in this section) c_{jk} is found by solving a set of linear algebraic equations (see Eq. (26)). To find a unique c_{jk} from the linear algebraic equations the number of unknowns, r in $(\tilde{\ddot{\boldsymbol{y}}}_d)_k = \sum_{j=0}^{r} c_{jk} e^{m_{jk} t}$, must be equal to the number of the equations resulting by imposing the conditions 3–1, 3–2 and 3–3 discussed in Section 5. Therefore, the required number of the exponential functions for each segment is:

$$r = 2(h+1) + nu \tag{31}$$

Here $2(h+1)$ equations come from the condition 3–1, Eq. (30). Also, nu equations are due to the continuity of $\boldsymbol{X}_I^u$ at the start of each segment (condition 3–3) where nu is the size of the vector $\boldsymbol{X}_I^u$; or equally nu is the number of unstable zeros of the transfer function (positive and purely imaginary zeros) considering the end-effector displacement as the output.

After determining the required number of the exponential functions from Eq. (31), the satisfaction of conditions 3–1 to 3–3 results in a relationship between c_{jk} and m_{jk} (see Eq. (26)). Therefore, if m_{jk} are given, c_{jk} can be obtained in terms of m_{jk} ($\bar{\boldsymbol{c}}_k = \boldsymbol{Z}_k{}^{-1}(\boldsymbol{C}_T)_k$). Thus, in the following a method for the selection of m_{jk} for each segment is introduced. This method is easy to implement and makes it possible to continue and explore the concept of piece-wise trajectory redefinition by SSEF which is the main focus of this paper. Other way of selecting m_{jk} can be found in [16].

Consider the exponential function:

$$y = ce^{mt} \quad m < 0 \tag{32}$$

which has to be calculated in the interval $t_i < t < t_f$. The decay of the exponential function, y in Eq. (32), at t_f with respect to its value at time t_i is:

$$C_{dec} = y(t_f)/y(t_i) = e^{mt_f}/e^{mt_i} \tag{33}$$

Assuming a value for the decay C_{dec}, in the specified time interval ($t_i < t < t_f$), the corresponding m is obtained by combining Eqs. (32) and (33), which is:

$$m = Ln(C_{dec})/(t_f - t_i) \tag{34}$$

Thus, if the fastest and slowest decays for the exponential functions used in the kth segment are assumed to be $(C_{dec}^f)_k$ and $(C_{dec}^s)_k$ respectively, the corresponding m from Eq. (34), are:

$$m_k^f = Ln(C_{dec}^f)_k/(t_{fk} - t_{ik}), \quad m_k^s = Ln(C_{dec}^s)_k/(t_{fk} - t_{ik}) \tag{35}$$

According to Eq. (29), the number of the m at each segment has to be the same as the number of the required exponential functions. Thus, having the required number of the exponential

functions for the kth segment from Eq. (31), and the slowest and the fastest m from Eq. (35) (after the selection of $(C^f_{dec})_k$ and $(C^s_{dec})_k$), the other m are chosen between m^f_k and m^s_k. To have the maximum difference between the m for the numerical stability of the solution of the linear equations [16], the other m are equally spaced between m^f_k and m^s_k. Therefore, the m for the kth segment are:

$$m_{jk} = m^s_k + \frac{m^f_k - m^s_k}{(r-1)}(j-1),\ j = 1,...,r \tag{36}$$

From Eqs. (35) and (36) it is clear that by selecting different pairs of $(C^f_{dec})_k$ and $(C^s_{dec})_k$ different values for m_{jk} can be obtained. Thus, the redefinition of the desired trajectory at each segment can be done in several different ways, which is a benefit of using the SSEF instead of the polynomial functions.

7. SIMULATION RESULTS

To show the effectiveness of the proposed method for different cases of linear nonminimum phase systems, simulation examples for three different SFLM were performed. These examples were:

1- a SFLM with a non-hyperbolic internal dynamics; that is, there were purely imaginary zeros for the transfer function (or equally there are purely imaginary eigenvalues for matrix $\mathbf{A}_I$ in Eq. (14)).

2- a SFLM with a near non-hyperbolic internal dynamics, which meant that its transfer function had zeros that were close to the imaginary axis; and

3- a SFLM with a hyperbolic internal dynamics and therefore it did not have any purely imaginary zeros or zeros that were close to the imaginary axis.

In the following the results of the first simulation, a SFLM with a non-hyperbolic internal dynamics which is the most challenging one [11], is presented and the results of the second and third simulations are not reported for briefness. However, the results for the second and third simulations (SFLM with near non-hyperbolic internal dynamics and hyperbolic internal dynamics, respectively) are available in Chapter 2 in [15].

For the first simulation, a SFLM with the physical properties given in table 1 was considered. This SFLM had the same physical parameters as in [10]. Moreover, the flexibility of the link was modeled with the first two flexible modes. The zeros of the transfer function which are the eigenvalues of matrix $\mathbf{A}_I$ in Eq. (14) were ± 61.25 and $\pm 54.34i$. Since the transfer function of the SFLM had purely imaginary zeros $\pm 54.34i$, the internal dynamics was non-hyperbolic and the inversion introduced in [6,8,9] was not possible [11]. However, the method described here can handle purely imaginary zeros.

For comparison, the desired end-effector displacement for this example, as shown in Fig. 3, was taken exactly from [10]. This trajectory was obtained using a polynomial for the planned output and assuming the following initial and final conditions (details can be found in [10]):

Table 1 Simulation, physical properties of the SFLM

$L(m)$	$EI(N.m^2)$	$I_h(kg.m^2)$	$\rho(kg/m)$	$I_{tip}(kg.m^2)$	$m_{tip}(kg)$
1.005	47.25	1.800×10^{-3}	2.032	4.742×10^{-2}	6.790

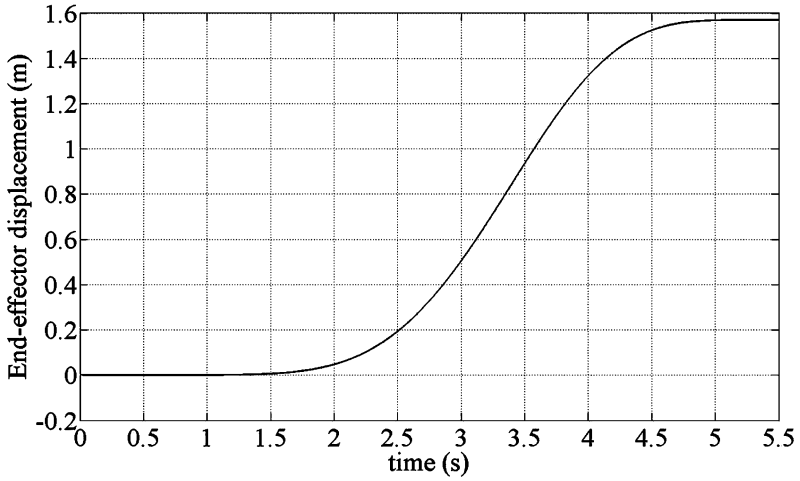

Fig. 3. Simulation, desired end-effector displacement

$$\begin{cases} y(5.50)=1.57(m),\ y(0)=\dot{y}(0)=\ddot{y}(0)=\ddot{y}^{(1)}(0)=\ddot{y}^{(2)}(0)=\ddot{y}^{(3)}(0)=0.0 \\ \dot{y}(5.5)=\ddot{y}(5.5)=\ddot{y}^{(1)}(5.5)=\ddot{y}^{(2)}(5.5)=\ddot{y}^{(3)}(5.5)=0.00 \end{cases} \tag{37}$$

where $\ddot{y}^{(h)}=d^h\ddot{y}/dt^h=d^{(h+2)}y/dt^{(h+2)}$. The reason for selecting this trajectory is as follows. In [10] the trajectory, as given in Fig. 3, was obtained by adopting a point-to-point manoeuvre. However, the problem here was to follow a desired trajectory as opposed to a point-to-point motion. Therefore, the trajectory given in [10] and also shown in Fig. 3, was assumed as the desired trajectory and the piece-wise causal inversion was used to follow this trajectory. Thus, the required causal torques have to be the same here and in [10]. By comparing the torque in Fig. 4 and that obtained in [10], it was seen that these torques are in fact the same. This comparison can serve as a check for the validity of our new method.

Since the input to the inverse equations was the second derivative of the desired end-effector displacement, Eqs. (14), the acceleration of the end-effector was redefined by SSEF. Therefore,

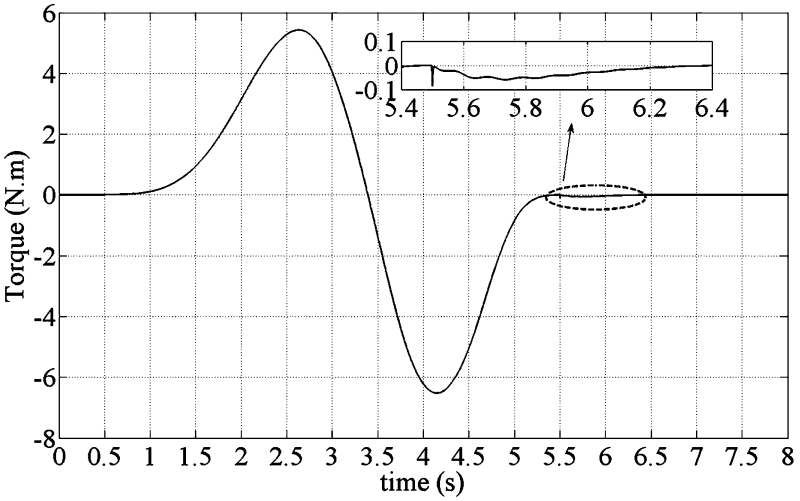

Fig. 4. Simulation, required base torque for causal end-effector trajectory inversion of the SFLM

the desired end-effector acceleration derived from the desired end-effector displacement was divided into 5 equal segments which were:

$$0.00 \le t \le 1.1,\ 1.1 \le t \le 2.2, \ldots..,\ 4.4 \le t \le 5.5 \tag{38}$$

It was assumed that $h=2$ (see condition 3–1 in Section 5). Moreover $nu = 3$ since there were three unstable zeros; +61.25 and $\pm 54.34i$. Therefore, the number of exponential functions for each segment was $r = 9$ from Eq. (31). Also, the "m" for each segment were derived using Eqs. (35) and (36) and assuming:

$$(C^f_{dec})_k = 0.0001 \quad (C^s_{dec})_k = 1.000 \tag{39}$$

Due to the redefinition of the acceleration, the end-effector velocity at the end of the manoeuvre would not necessary be zero and the final position of the end-effector might be different from the desired one. The closer the redefined acceleration is to the desired acceleration, the smaller will be the difference. However, the addition of a joint PD controller to the nominal input torque, derived by piece-wise causal inversion, not only makes the closed loop control robust but also reduces these errors to zero and suppresses the link's vibration [17]. Therefore, the input torque to the dynamic model was set to:

$$\tau = \tau_l + k_P(\theta_d - \theta) + k_D(\dot{\theta}_d - \dot{\theta}) \tag{40}$$

where τ_l was the piece-wise causal torque calculated from the inversion of the linear dynamic equation, Eq. (8), k_P and k_D were the scalar gains, and θ_d and $\dot{\theta}_d$ were the redefined desired joint rotation and velocity, respectively. In this example, the torque obtained from Eq. (40) was applied to the SFLM. After 5.5 (s), the computed inverse dynamic torque, τ_l in Eq. (40), was set to zero and only the joint PD controller, assuming the desired joint rotation stay constant at $y_d(t_f)/L = 1.56$(rad), was active. The stability of the proposed controller is given in Section 2 in [15].

In Fig. 4, the simulation torque employing $k_P = 15$ and $k_D = 30$ is shown. These gains were obtained by trial and error observing the system's response (relatively fast settling time and

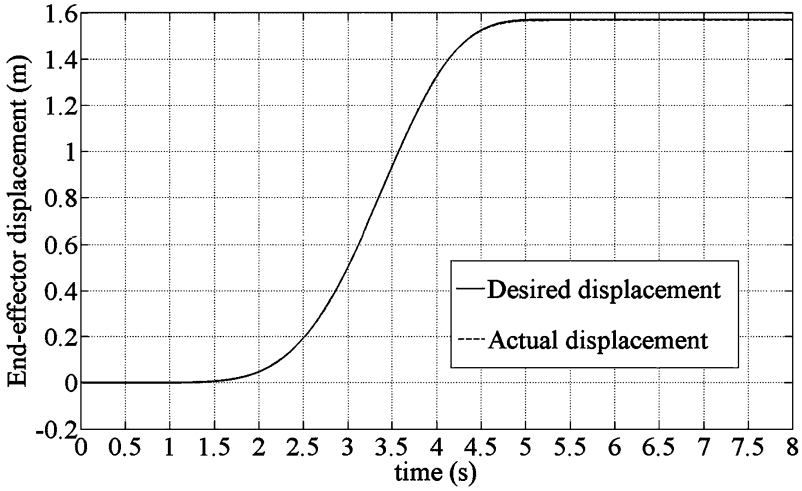

Fig. 5. Simulation, desired and actual end-effector displacements for the SFLM

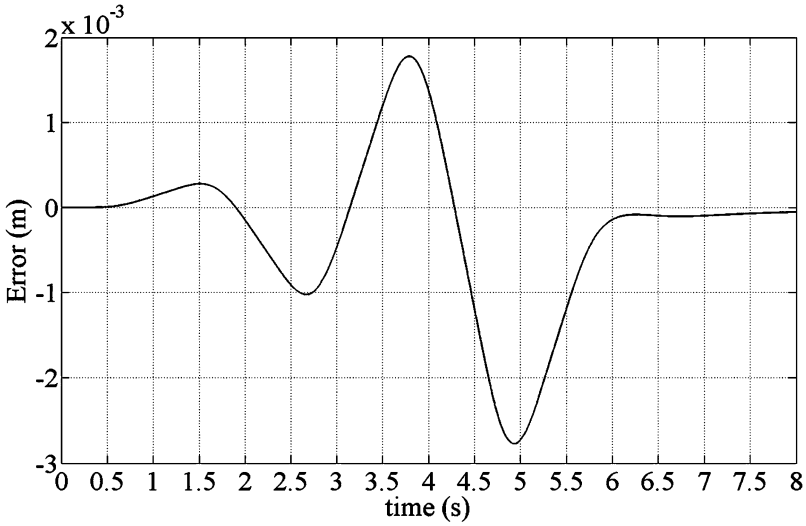

Fig. 6. Simulation, the difference between the actual and desired end-effector displacements of the SFLM which are shown in Fig. 5

small overshoot) and also noting that k_P and k_D had to be selected so that they guarantee a stable closed-loop system. Details on how these gain selected and why they satisfy the closed-loop stability can be found in [15]. The small value of the torque after 5.5 (s) was due to the joint PD controller. Moreover, it was observed that the torque was discontinuous at 5.5 (s), as expected. This was due to the fact that after 5.5 (s) the off-line inverse torque was set to zero and only the joint PD controller was active. In Fig. 5, the desired and actual end-effector displacements are shown. In Fig. 6, the difference between the actual and desired end-effector displacements, $error = y_d - y$, is shown. As can be seen after 5.5 (s) due to the PD controller, the actual displacement approached the desired displacement.

Remark 2: To make the torque discontinuity at the end of the manoeuvre approach zero, the desired trajectory in the last segment can be redefined so that, at the end of the manoeuvre, t_f, not only the redefined displacement and its velocity have the same values as their desired ones but also the link's deflection due to the link flexibility and its velocity are set to be zero, which is under study and preliminary results are available in [16,18]. Therefore, after applying the torque obtained by the inversion process to the dynamic model, the manipulator comes to rest at the end of the manoeuvre, for a rest-to-rest motion, while the end-effector moves along a desired path.

Fig. 7. The SFLM in the Robotics Laboratory at U of S (University of Saskatchewan)

8. EXPERIMENTAL RESULTS

To show the feasibility of the introduced technique, in this section the results of an experimental study are presented. The SFLM in Fig. 7 which is available at the robotic laboratory of the University of Saskatchewan (U of S) was used for this experimental verification. The simulation results for this experiment are available in [15] and not reported here for briefness.The flexible link of the SFLM in Fig. 7, was made of stainless steel with a length of 0.2300 (m), a thickness of 8.890×10^{-4} (m) and a width of 0.0381(m). The mass moment of inertia of the hub was 0.0198 (kg.m^2), and the coefficient of viscous damping was 0.3200 (N.m.s/rad). Moreover, the SFLM had a payload at the tip with the mass of 0.1690 (kg) and a mass moment of inertia of 2.570×10^{-5}(kg.m^2). In addition, there was a high rotational dry friction in the experimental setup due to the employed harmonic drive. This friction is refereed to as joint dry friction. The existence of this joint dry friction, which is hard to model exactly [19], deteriorates the performance of the model based controllers [20]. In this paper, like in [21], to compensate for the friction, the average value of the joint dry friction was measured and added to the control torque in Eq. (40). This average value of the joint dry friction was obtained experimentally by applying a step input torque to the motor and recording the joint angular velocity versus time (velocity profile). Repeating this experiment gave different velocity profiles for different values of the step input torques. Since the closed-form function of the velocity profile for a step input torque is known, by using a curve fitting scheme the average value of the joint dry friction was obtained which was 0.45 (N.m).

For the experimental study, the link flexibility was modeled with the first mode shape of vibration, since the maximum bandwidth of the actuator was smaller than the second natural frequency. The maximum actuator bandwidth was 50 (Hz) [22] while the natural frequency of the second mode was 54 (Hz). Therefore, the first mode of vibration was dominant and the contributions of the second and higher modes of vibration were minimal, which justified modeling the link with only one mode. Generally, for a typical SFLM (or even multilink flexible manipulator) contributions of the higher modes of vibration are very small. This was also observed in the simulation examples and also in the results of [14,23] for bang-bang torques and was believed to be the main reason why in previous experimental studies of controllers [24,25]

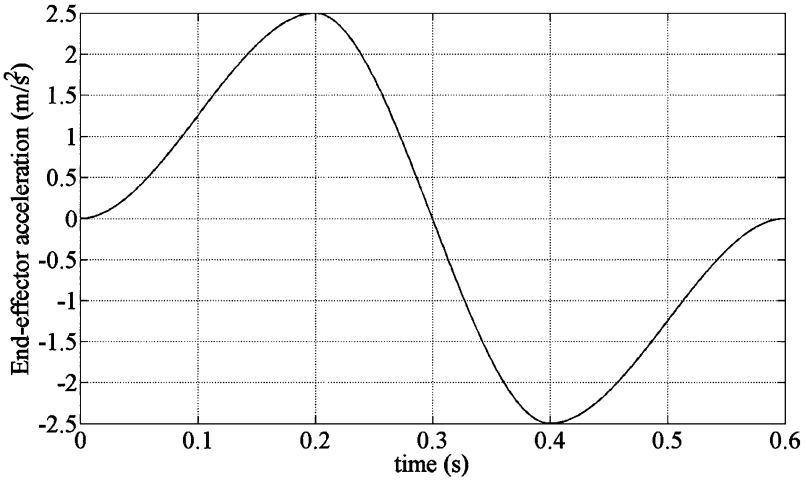

Fig. 8. Experimental, desired end-effector acceleration of the SFLM in Robotics Laboratory at the U of S

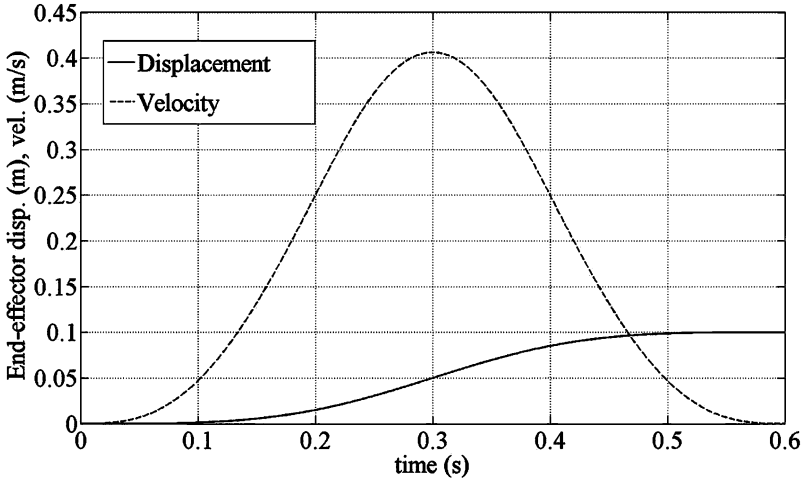

Fig. 9. Experimental, desired end-effector velocity and displacement of the SFLM in the Robotics Laboratory at the U of S

only one mode shape per link had been used. By modeling the link flexibility with the first mode, the zeros of the corresponding transfer function were at ± 212.0. Thus, this SFLM was a nonminimum phase system with hyperbolic internal dynamics.

The desired end-effector acceleration, shown in Fig. 8, was considered which was composed of several third order polynomials, from 0 to 0.2, 0.2 to 0.4, and 0.4 to 0.6 (s). The corresponding desired velocity and displacement are presented in Fig. 9. The desired end-effector acceleration was divided into 6 equal segments which were:

$$0.0 \le t \le 0.1,\ 0.1 \le t \le 0.2, \ldots..,\ 0.5 \le t \le 0.6 \tag{41}$$

and in each segment the desired acceleration was redefined by SSEF. Similar to simulation example, $h = 2$ was selected in Eq. (30). Moreover, since there was only one unstable zero 212, *nu* was equal to 1. Using Eq. (31), the required number of exponential functions for each segment was $r = 7$. Also "m" for each segment was selected using Eqs. (35) and (36) and assuming $(C^f_{dec})_k = 0.0100$ and $(C^s_{dec})_k = 1.000$. The value of $(C^f_{dec})_k$ and $(C^s_{dec})_k$ were selected to be different in the simulation study than experimental study. The possibility of selecting these variables differently is the main advantage of using SSEF, since different values of $(C^f_{dec})_k$ and $(C^s_{dec})_k$ result in different redefined trajectories and torques. Thus, the control engineer can select theses parameters so that the required design criteria are met. In the simulation study $(C^f_{dec})_k$ and $(C^s_{dec})_k$ were found by trial and error so that the difference between the redefined and desired trajectories was minimized. In the experimental study not only minimizing this difference was of concern but also the maximum torque that can be applied by actuator was also considered in the trial and error procedure of finding $(C^f_{dec})_k$ and $(C^s_{dec})_k$.

The off-line inverse torque was combined with the joint PD controller, Eq. (40), and to compensate for the joint dry friction the average value of the joint dry friction, 0.45 (N.m), was added to it. After 0.6 (s) only the joint PD controller with $\theta_d = y_d(t_f)/L$ and $\dot{\theta}_d = 0$ was active. The gains of the PD controller were $k_P = 1.4$ and $k_D = 0.40$. These gain were obtained by trial and error such that (*i*)- the stability of the closed-loop system was guaranteed (*ii*)- the closed-loop system had acceptable performance which was relatively fast settling time and small overshoot. Details for the selection of these gains can be found in [15]. The results of this experimental are

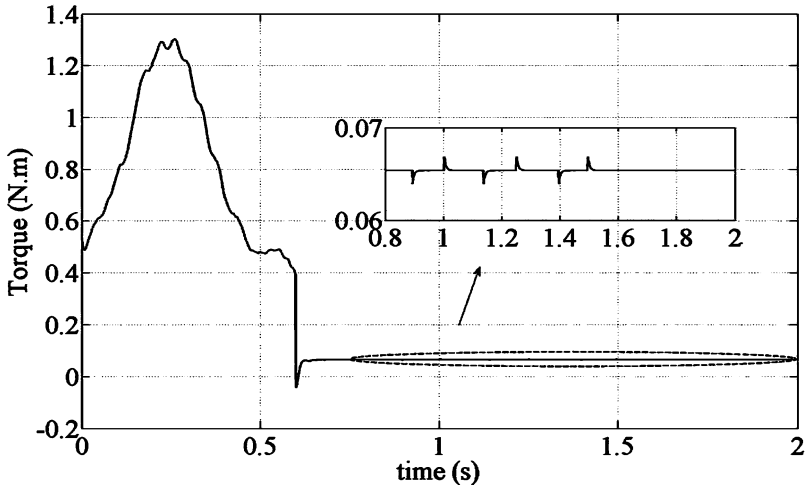

Fig. 10. Experimental, required base torque for causal end-effector trajectory tracking of the SFLM in the Robotics Laboratory at the U of S *without* authors' two-stage controller

shown in Figs. (10–12). The reason for having the wording "*without authors' two-stage controller*" in the captions of these figures will be clear in the following.

From Fig. 12, it was clear that a steady trajectory tracking error, about 0.01 (m), existed. Therefore, the joint PD controller by itself could not eliminate the steady trajectory tracking error. From Fig. 10 it was clear that after $t_f = 0.6$ (s), the actuator applied a constant torque. This torque was due to the existence of the steady tracking error, about 0.01(m), and the joint PD controller. Since the value of this torque was less than the joint dry friction, it could not rotate the hub and reduce the steady tracking error to zero. By increasing the gains of the PD controller, the constant value of the steady torque would increase and then overcome the joint dry friction. Nevertheless, implementing a joint PD controller, in the presence of friction, eventually leads to a steady tracking error in which the higher the PD gains, the smaller becomes the error. But using a PD controller with larger gain not only increases the sensitivity of the controller to noise but also lead to torque saturation and is not a rational remedy.

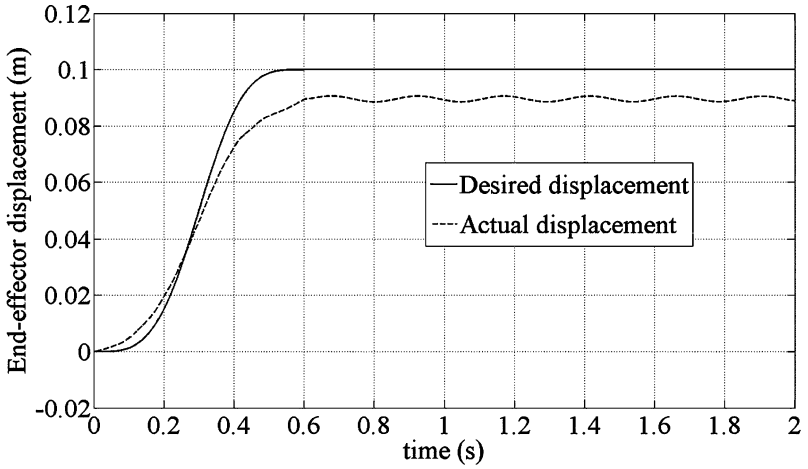

Fig. 11. Experimental, desired and actual end-effector displacements for the SFLM in the Robotics Laboratory at the U of S *without* the author's two-stage controller

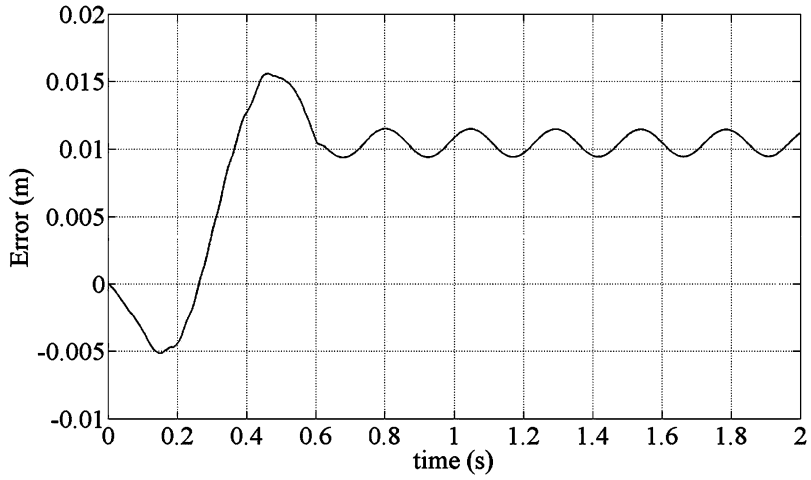

Fig. 12. Experimental, the difference between the actual and desired end-effector displacement of the SFLM in the Robotics Laboratory at the U of S which are shown in Fig. 11

To compensate for joint dry friction, a new two-stage controller is proposed. The utilization of this new controller does not indicate inefficiency of the new causal inversion end-effector controller introduced here. However, since the causal end-effector inversion is a model based controller and joint friction is not exactly known, a different controller is necessary to reduce the error to zero at the end of manoeuvre. Based on this proposed controller for the first stage, up to $t_f = 0.6$ (s), a constant torque of 0.45 (N.m) was added to the torque given is Eq. (40) and applied to the SFLM (as before). For the second stage, for $t > t_f$, the pulse width control (PWC) [26] was used to reduce the steady state error of the hub to zero (details of the PWC controller can be found in [15]). The schematic of this new two-stage controller is shown in Fig. 13.

The torque applied to the experimental SFLM using this two-stage controller is presented in Fig. 14. The actual and desired displacements and their differences $error = y_d - y$ using this new controller are shown in Figs. 15 and 16. Comparing Fig. 16, with Fig. 12 showed that the steady tracking error was reduced essentially due to the new two-stage controller. That is, the steady state trajectory tracking error was reduced from about 0.010 (m) to about 0.001 (m).

Figs. 15 and 16 show that there existed a slowly vanishing vibration of the manipulator. When the hub reached $0.1/L$ (rad) if the link vibration was suppressed, the steady end-effector trajectory tracking vanished. However, after applying the PWC there was no controller to

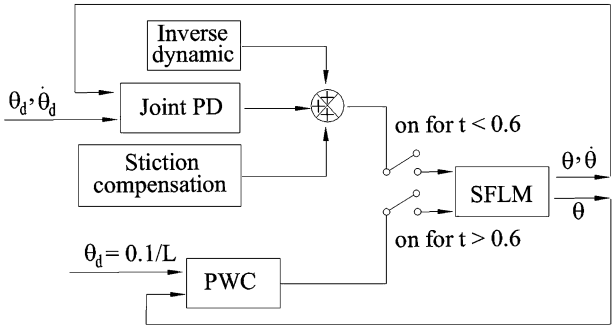

Fig. 13. Experimental, schematic of the author's two-stage controller used to eliminate the steady trajectory tracking error

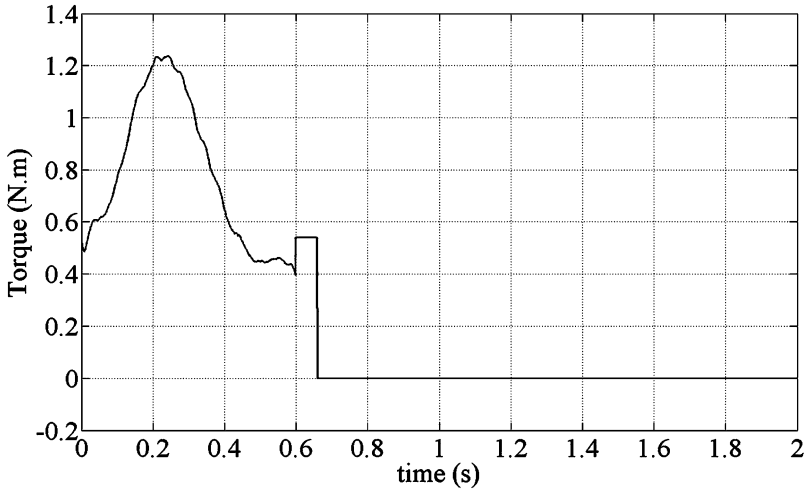

Fig. 14. Experimental, required base torque for causal end-effector trajectory tracking of the SFLM in the Robotics Laboratory at the U of S after using the authors' two-stage controller

suppress the vibration except the link's internal damping. While relying on the link's material damping for eliminating the vibration was not always satisfactory, the only available experimental SFLM setup in our Robotics Laboratory had this limitation. Even using the joint PD controller would not eliminate this little vibration at the end of manoeuvre because of the high value of the joint dry friction. The application of the piezoelectric actuator to overcome this drawback was among the possible solutions which are currently under study [27].

9. CONCLUSIONS

A novel causal end-effector trajectory inversion of a Single Flexible Link Manipulator (SFLM) by means of output redefinition has been introduced. The desired trajectory is divided into a finite number of segments, and each segment is redefined so that a bounded causal

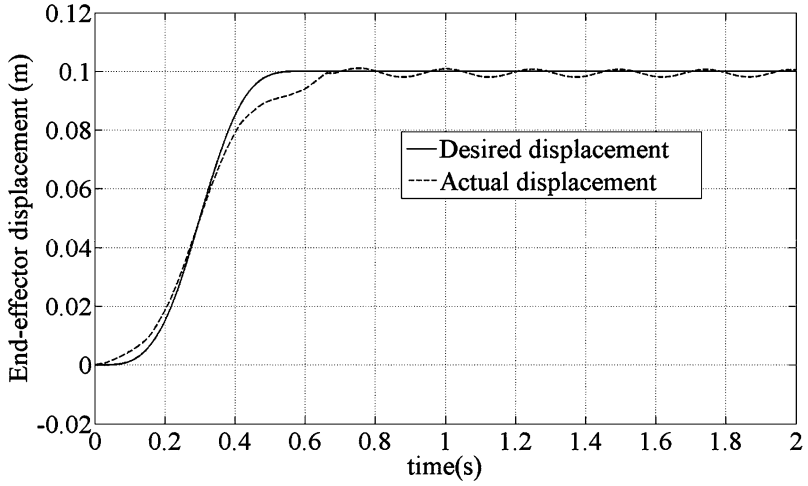

Fig. 15. Experimental, desired and actual end-effector displacements for the SFLM in the Robotics Laboratory at the U of S after using the authors' two-stage controller

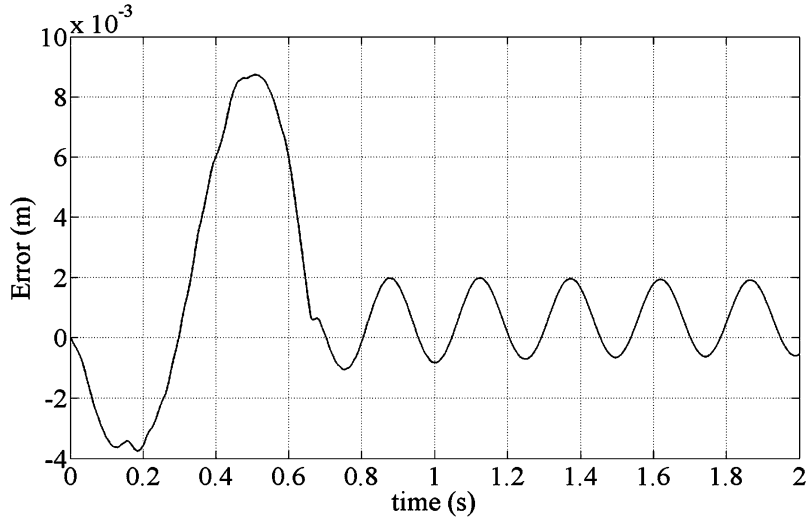

Fig. 16. Experimental, the difference between the actual and desired end-effector trajectories of the SFLM in the Robotics Laboratory at the U of S which are shown in Fig. 15

continuous inversion torque can be found. The redefinition of the desired trajectory employed stable exponential functions which lead to a family of possible solutions. Thus, the control engineer can choose that member of this family of possible solutions which best meets the required design criteria.

Although the available non-causal end-effector inversion technique did not tolerate existence of purely imaginary zeros for the transfer function between end-effector displacement and applied torque, the proposed method in this paper is still valid even in the presence of purely imagery zeros. The off-line computed inverse dynamic torque was combined with a joint PD controller and the stability of the proposed controller was investigated. The simulation results for SFLMs with hyperbolic, non-hyperbolic and near non-hyperbolic internal dynamics, which was without purely imaginary zeros, with purely imaginary zeros and zeros which were close to the imaginary axis respectively, were performed. The experimental results showed the feasibility of the introduced method. In the experimental study, due to the existence of the joint dry friction, a new two-stage controller was used to reduce the trajectory tracking error close to zero. While the method was studied here for the inversion of a SFLM, its extension to the causal inversion of linear single input single output, non-minimum phase systems with hyperbolic, non-hyperbolic or near non-hyperbolic internal dynamics is straight forward.

ACKNOWLEDGEMENTS

Financial support for this study was provided by a NSERC Discovery Grant. The authors would also like to express their gratitude toward the reviewers for their valuable comments.

REFERENCES

1. Wang, D. and Vidyasagar, M., "Transfer Function for a Single Flexible Link," *Proceedings of the IEEE International Conference on Robotics Automation*, Arizona, USA, 2, pp. 1042–1047, 1989.

2. Spector, V.A. and Flashner, H., "Modeling and Design Implications of Noncollocated Control in Flexible Systems," *Journal of Dynamic Systems, Measurement and Control*, Vol. 112, No. 2, pp. 186–193, 1990.
3. Park, J.H. and Asada, H., "Dynamic Analysis of Noncollocated Flexible Arms and Design of Torque Transmission Mechanisms," *Journal of Dynamic Systems, Measurement and Control*, Vol. 116, No. 2, pp. 201–207, 1994.
4. Isidori, A. and Byrnes, C., "Output Regulation of Nonlinear System," *IEEE Transactions on Automation and Control*, Vol. 35, No. 2, pp. 131–140, 1990.
5. De Luca, A., Lanari, L. and Ulivi, G., "Tip Trajectory Tracking in Flexible Arms: Comparison of Approaches Based on Regulation Theory," *Lecture Notes in Control and Information Sciences*, Vol. 162, pp. 190–206, 1991.
6. Devasia, S., Chen, D. and Paden, B., "Nonlinear Inversion-Based Output Tracking," *IEEE Transactions on Automatic Control*, Vol. 41, No. 7, pp. 930–942, 1996.
7. Slotine, J.J. and Li, W., *Applied Nonlinear Control*, Prentice Hall, NJ, USA, 1991.
8. Bayo, E., "A Finite-Element Approach to Control the End-Point Motion of a Single Link Flexible Robot," *Journal of Robotic Systems*, Vol. 4, No. 1, pp. 63–75, 1989.
9. Kwon, D.S. and Book, W.J., "Time-Domain Inverse Dynamic Tracking Control of a Single-Link Flexible Manipulator," *Journal of Dynamic Systems, Measurement and Control*, Vol. 116, No. 2, pp. 193–200, 1994.
10. Bensoman, M. and LeVey, G., "Stable Inversion of SISO Nonminimum Phase Systems through Output Planning: An Experimental Application to the One-Link Flexible Manipulator," *IEEE Transactions on Control Systems Technology*, Vol. 11, No. 4, pp. 588–597, 2003.
11. Devasia, S., "Approximated Stable Inversion for Nonlinear System with Nonhyperbolic Internal Dynamics," *IEEE Transactions on Automatic Control*, Vol. 44, No. 7, pp. 1419–1425, 1999.
12. Vakil, M., Fotouhi, R. and Nikiforuk, P.N., "Causal Inversion of a Single-Link Flexible Link Manipulator via Output Planning," *Proceedings of the IEEE International Conference on Mechatronics and Automation*, Niagara Falls, Ontario, Canada, pp. 376–381, 2005.
13. Book, W.J., "Recursive Lagrangian Dynamic of Flexible Manipulator Arms," *International Journal of Robotics Research*, Vol. 3, No. 3, pp. 87–101, 1984.
14. Vakil, M., Fotouhi, R., Nikiforuk, P.N. and Salmasi, H., "A Constrained Lagrange Formulation of Multi-link Planar Flexible Manipulator," *Journal of Vibration and Acoustics*, Vol. 130, No. 3, pp. (0300017) 1–16, 2008.
15. Vakil, M., "Dynamics and Control of Flexible Manipulators," *Ph.D. Dissertation*, University of Saskatchewan, Canada, 2008.
16. Vakil, M., Fotouhi, R. and Nikiforuk, P.N., "End-effector Inversion of Flexible Manipulators," *Mechatronics*, revised version resubmitted, Doi:10.1016/j.mechatronics.2009.03.010, 2009.
17. Yigit, A.S., "On the Stability of PD Control for a Two-Link Flexible Manipulator," *Journal of Dynamic Systems, Measurement and Control*, Vol. 116, No. 2, pp. 208–215, 1994.
18. Vakil, M., Fotouhi, R. and Nikiforuk, P.N., "End-Effector Trajectory Inversion of a Single Flexible Link Manipulator With Non-Zero Initial States," *Proceeding of the 16th IASTED International Conference on Applied Simulation and Modeling*, Palma de Malorca, Spain, pp. 485–490, 2007.
19. de Wit, C.C., Olsson, H., Astrom, K.J. and Lischinsky, P., "A New Model for Control of System with Friction," *IEEE Transactions on Automatic Control*, Vol. 40, No. 3, pp. 419–425, 1995.
20. Armstrong-Helouvry, B., *Control of Machines with Friction*, Kluwer, MA, USA, 1993.

21. Gandhi, P.S. and Chorbel, F.H., "Closed Loop Compensation of Kinematic Error in Harmonic Drives for Precision Control Application," *IEEE Transactions on Control Systems Technology*, Vol. 10, No. 6, pp. 759–768, 2002.
22. Reference Manual, 2-DOF Serial Flexible Link Robot, www.quanser.com
23. Luca, A.D. and Siciliano, B., "Closed-Form Dynamic Model of Planar Multilink Lightweight Robots," *IEEE Transactions on Systems, Man and Cybernetics*, Vol. 21, No. 4, pp. 826–839, 1991.
24. Moallem, M., Patel, R.V. and Khorasani, K., "Nonlinear tip-position Control of a Flexible-Link Manipulator: theory and experiments," *Automatica*, Vol. 37, pp. 1825–1834, 2001.
25. Cheong, J., Chung, W.K. and Youm, Y., "Inverse Kinematics of Multilink Flexible Robots for High-Speed Application," *IEEE Transactions on Robotics and Automation*, Vol. 20, No. 2, pp. 269–282, 2004.
26. Rathbun, D.B., Berg, M.C. and Buffinton, K.W., "Pulse Width Control for Positioning of Structurally Flexible Systems Subjected to Stiction and Coulomb Friction," *Journal of Dynamic Systems, Measurement and Control*, Vol. 126, No. 1, pp. 126–138, 2004.
27. Salmasi, H., Fotouhi, R. and Nikiforuk, P.N., *Active Vibration Suppression of a Flexible Link Manipulator Using Piezoelectric Actuator*, Computer Aided Optimum Design in Engineering, WIT Press, pp. 199–208, 2007.

NOMENCLATURE

$\mathbf{A}$	State matrix when the dynamic model is represented in the state space form
$\mathbf{A}_I$	State matrix of the internal dynamics
$\mathbf{A}_I^-$ $(\mathbf{A}_I^+)$	Diagonal matrix representing the eigenvalues of $\mathbf{A}_I$ with negative (positive) real parts
$\boldsymbol{B}$	Input matrix when the dynamic model is represented in the state space form
$\boldsymbol{B}_I$	Input matrix of the internal dynamics
$\boldsymbol{B}_I^u$	Input matrix corresponding to $\mathbf{A}_I^+$
$\boldsymbol{B}_I^s$	Input matrix corresponding to $\mathbf{A}_I^-$
$\boldsymbol{C}$	Output matrix of the dynamic model in state space
$\mathbf{C}_D$	Damping matrix
C_{dec}	Decay of an exponential function
$(C_{dec}^f)_k$	The fastest decay for the exponential functions in the kth segment
$(C_{dec}^s)_k$	The slowest decay for the exponential functions in the kth segment
$\mathbf{C_{cc}}(\dot{\boldsymbol{\theta}},\boldsymbol{\lambda},\dot{\boldsymbol{\lambda}})$	Matrix of the Coriolis and the centrifugal forces in the lateral direction
EI	Rigidity of a flexible link
$\boldsymbol{F}$	Force vector
I_{tip}	Mass moment of inertia of the tip payload
I_h	Mass moment of inertia of the hub
$\mathbf{K}_B$	Stiffness matrix
k_P	Proportional gain of PD controller
k_P	Derivative gain of PD controller
L	Length of flexible link
$\mathbf{M}(\boldsymbol{\lambda})$	Mass matrix
m	Exponent of exponential function
m_{jk}	The jth m in the kth segment

m_k^f	Value of m corresponding to $(C_{dec}^f)_k$
m_k^s	Value of m corresponding to $(C_{dec}^s)_k$
m_{tip}	Mass of payload at tip
n	Number of assumed mode shapes used in $\xi(\gamma,t)$
nu	Size of vector$\boldsymbol{X}_I^u$
$\boldsymbol{q}$	Vector of the generalized coordinates for SFLM
r	Required number of exponential functions
t_f	Final manoeuvre time
t_{ik}	Initial time of the kth segment
t_{fk}	Final time of the kth segment
ω	Fundamental natural frequency of SFLM
$\boldsymbol{X}_I$	State vector of the internal dynamics
$\boldsymbol{X}_I^u$	State vector corresponding to $\mathbf{A}_I^+$
$\boldsymbol{X}_I^s$	State vector corresponding to $\mathbf{A}_I^-$
y	End-effector displacement (position)
y_d	Desired end-effector trajectory
$(\ddot{y}_d)_k$	$\ddot{y}_d$ in the kth segment
$\tilde{y}_d(t)$	Redefined trajectory
$y_p(t)$	The polynomial function
τ	Input torque
$\xi(\gamma,t)$	Spatial deflection of the flexible link
$\phi_j(\gamma)$	The jth spatial pre-defined shape function
$\lambda_j(t)$	Time varying weight function of $\phi_j(\gamma)$
$\boldsymbol{\lambda}$	Vector of $\lambda_j(t)$ elements
η	Damping ratio
θ	Joint rotation of SFLM
ρ	Mass per unit length